

Toward PET/MRI as one-stop shop for radiotherapy planning in cervical cancer patients

Sahar Ahangari^a , Naja Liv Hansen^a, Anders Beck Olin^a, Trine Jakobi Nøttrup^b, Heidi Ryssel^a, Anne Kiil Berthelsen^a, Johan Löfgren^a, Annika Loft^a, Ivan Richter Vogelius^b , Tine Schnack^{c,d}, Bjoern Jakoby^e, Andreas Kjaer^{a,f}, Flemming Littrup Andersen^{a,g}, Barbara Malene Fischer^{a,g,h,*}  and Adam Espe Hansen^{a,g,i,*}

^aDepartment of Clinical Physiology, Nuclear Medicine and PET, Rigshospitalet, University of Copenhagen, Copenhagen, Denmark; ^bDepartment of Oncology, Section of Radiotherapy, University of Copenhagen, Rigshospitalet, Denmark; ^cDepartment of Gynecology, University of Copenhagen, Copenhagen, Denmark; ^dDepartment of Gynecology and Obstetrics, Odense University Hospital, Odense, Denmark; ^eSiemens Healthcare Sector, Erlangen, Germany; ^fCluster for Molecular Imaging, University of Copenhagen, Copenhagen, Denmark; ^gDepartment of Clinical Medicine, University of Copenhagen, Copenhagen, Denmark; ^hThe PET Centre, School of Biomedical Engineering and Imaging Sciences, Kings College London, St Thomas' Hospital, London, UK; ⁱDepartment of Diagnostic Radiology, Rigshospitalet, University of Copenhagen, Denmark Copenhagen

ABSTRACT

Background: Radiotherapy (RT) planning for cervical cancer patients entails the acquisition of both Computed Tomography (CT) and Magnetic Resonance Imaging (MRI). Further, molecular imaging by Positron Emission Tomography (PET) could contribute to target volume delineation as well as treatment response monitoring. The objective of this study was to investigate the feasibility of a PET/MRI-only RT planning workflow of patients with cervical cancer. This includes attenuation correction (AC) of MRI hardware and dedicated positioning equipment as well as evaluating MRI-derived synthetic CT (sCT) of the pelvic region for positioning verification and dose calculation to enable a PET/MRI-only setup.

Material and methods: 16 patients underwent PET/MRI using a dedicated RT setup after the routine CT (or PET/CT), including eight pilot patients and eight cervical cancer patients who were subsequently referred for RT.

Data from 18 patients with gynecological cancer were added for training a deep convolutional neural network to generate sCT from Dixon MRI. The mean absolute difference between the dose distributions calculated on sCT and a reference CT was measured in the RT target volume and organs at risk. PET AC by sCT and a reference CT were compared in the tumor volume.

Results: All patients completed the examination. sCT was inferred for each patient in less than 5 s. The dosimetric analysis of the sCT-based dose planning showed a mean absolute error (MAE) of 0.17 ± 0.12 Gy inside the planning target volumes (PTV). PET images reconstructed with sCT and CT had no significant difference in quantification for all patients.

Conclusions: These results suggest that multiparametric PET/MRI can be successfully integrated as a one-stop-shop in the RT workflow of patients with cervical cancer.

ARTICLE HISTORY

Received 15 February 2021
Accepted 23 May 2021

KEYWORDS

PET/MR hybrid imaging; RT treatment planning; dose calculation; PET attenuation correction; DL-based synthetic CT

Background

Cervical cancer is common cancer affecting middle-aged women [1]. Two types of radiation therapy (RT) constitute the cornerstone of initial treatment: external beam radiation therapy (EBRT) and brachytherapy (BT) [2–4]. Despite recent improvement in therapeutic ratio, the incidence of recurrence in cervical cancer is approximately 25% [1,5]. The application of advanced RT techniques significantly improves the safe delivery of increased doses to the target volume while sparing the adjacent normal tissue and critical organs [6,7]. Therefore, optimized methods are required for more accurate

delineation of the clinical target volume (CTV) and organs at risk (OAR).

In RT planning, computed tomography (CT) remains the primary imaging modality for patient positioning and a prerequisite for dose calculations. For patients with cervical cancer, target volume delineation mainly relies on magnetic resonance imaging (MRI) due to its high soft-tissue contrast [8]. The application of positron emission tomography (PET), as well as modern functional MRI techniques, can noninvasively visualize different aspects of tumor biology [9–11]. However, systematic registration errors between planning CT and other modalities can have a major impact upon the

CONTACT Sahar Ahangari  sahar.ahangari@regionh.dk  Department of Clinical Physiology, Nuclear Medicine and PET, Rigshospitalet, University of Copenhagen, Copenhagen, Denmark

*B. M. Fischer and A. E. Hansen should be considered joint senior authors.

© 2021 The Author(s). Published by Informa UK Limited, trading as Taylor & Francis Group.
This is an Open Access article distributed under the terms of the Creative Commons Attribution-NonCommercial-NoDerivatives License (<http://creativecommons.org/licenses/by-nc-nd/4.0/>), which permits non-commercial re-use, distribution, and reproduction in any medium, provided the original work is properly cited, and is not altered, transformed, or built upon in any way.

delivered dose to the target volume. Therefore, integration of multi-parametric PET/MRI into a one-stop-shop RT planning workflow of patients with cervical cancer could be a powerful strategy to improve target definition, while minimizing inter-modality registration errors and the number of examinations [12].

However, replacing CT and MRI with a combined PET/MRI for RT planning still remains challenging [13,14]. MRI images are typically affected by geometric distortion, which may also be induced by the PET components [15]. This is particularly problematic for RT planning as it directly translates into inaccurate target volume delineation and dose calculation [16]. In addition, RT planning requires reproducible patient positioning during both imaging for treatment planning and throughout treatment. Thus, to enable PET/MRI-only treatment planning, patient-specific information about tissue composition is required as a reference image for position verification prior to the treatment [17]. CT is also essential to achieve accurate radiation dose calculation for radiotherapy [12,18,19]. Several approaches have recently been proposed to generate synthetic CT (sCT) from MR images [20–23]. However, MR-derived sCT is challenged by the variety of tissue types and bowel gas present in the pelvic region. Promising results have recently been achieved using deep learning (DL)-based methods, particularly convolutional neural network (CNN) [24–27], but most studies are focusing on MRI-only RT planning rather than PET/MRI [28–30]. This comes at the expense of the challenges associated with PET attenuation correction (AC) and fitting the RT equipment into the 60 cm bore size of current integrated PET/MRI systems. PET images need to be quantitatively correct in order to be clinically used for target volume delineation. Several methods were proposed to improve vendor-provided MR-AC method [31]. Nevertheless, PET/MRI lacks a clinically accepted standard AC method, as compared to PET/CT. In addition, positioning equipment and MRI hardware are significant sources of photon attenuation in hybrid PET/MRI systems and must be considered in the AC process [32,33]. RT equipment was first introduced for PET/MRI of the head and neck region [34] and later for PET/MRI imaging from head to abdomen [13]. However, the feasibility of a dedicated PET/MRI RT setup for the cervix has not yet been demonstrated.

The objective of this study was to investigate the full integration of hybrid PET/MRI functional imaging into RT planning of cervical cancer patients. This includes the technical challenges regarding attenuation correction of MRI hardware and RT positioning equipment as well as generating MR-derived sCT of the pelvic region for position verification, PET AC, and dose calculation.

Material and methods

Patients

This paper presents data from a total of 34 patients undergoing whole-body CT (or PET/CT) prior to regional PET/MRI of the pelvic region. These patients were included in three groups: (1) eight patients (pilot patients) were used to optimize the setup and the scan protocol. (2) for clinical

feasibility, another eight patients (study patients) with cervical cancer (FIGO stages \geq IB2-IVA) referred for treatment with radio-chemotherapy were included, and (3) scans from 18 patients with gynecological cancer (GC patients) plus the eight pilot patients were used as training data for synthesizing CT images. All patients gave written informed consent, and the study was approved by the local ethics committee (H-2-2012-128, H-18042903, H-16047996).

Treatment position: using dedicated RT equipment

Patients were positioned in the supine position, reproducible for later RT treatment, using a dedicated RT set up (Figure 1(A)) including a PET and MR compatible flat table overlay (Medibord Ltd.), designed for the Siemens Biograph mMR system. The table is equipped with a coil holder with a height of 25 cm that attaches to the semi-circular recessed indexing points on the table. A custom-made coil holder, 3.5 cm higher was used for larger patients. The coil holder was placed in one of the predefined positions to provide full coverage of the pelvic region.

The patient's arms were folded over their chest and both legs fixated using the dedicated MR compatible knee and feet fixation device (CombifixTM, CIVCO Medical Solutions).

Patient data acquisition

CT imaging

Prior to EBRT of the eight cervical cancer patients, planning CT was carried out on a stand-alone CT scanner (Somatom Definition, Siemens Healthineers) in RT treatment position. The CT scans were performed with a tube voltage of 120 kV and tube current of 170 mA.

CT images of the pilot and GC patients were acquired in routine position from a whole-body PET/CT examination (Siemens Biograph mCT, Siemens Healthineers) with intravenous (IV) contrast, as part of the clinical routine with a tube voltage of 120 kV and reference mAs of 240 using CareDose 4D.

PET/MRI imaging

PET/MRI examinations were carried out on a whole-body hybrid PET/MRI system (Biograph mMR, Siemens Healthineers). Study patients were scanned 30 min after injection of 200 MBq ⁶⁸Ga-NODAGA-E[c(RGDyK)]₂ (RGD), an in-house developed angiogenesis PET tracer [35], and PET data was acquired in list-mode over 1 bed position in 20 min acquisition time. One of the patients was not administered RGD due to tracer production issues. PET image reconstruction was performed offline (e7tool, Siemens Healthineers) using the 3D ordinary Poisson ordered-subset expectation maximization (3D OP-OSEM) algorithm, 3 iterations, and 21 subsets, and a Gaussian filter with 4 mm full width at half maximum (FWHM).

Simultaneously with PET, T1, and T2 weighted turbo-spin echo (TSE) sequences were acquired along with the standard axial Dixon-VIBE (volumetric interpolated breath-hold

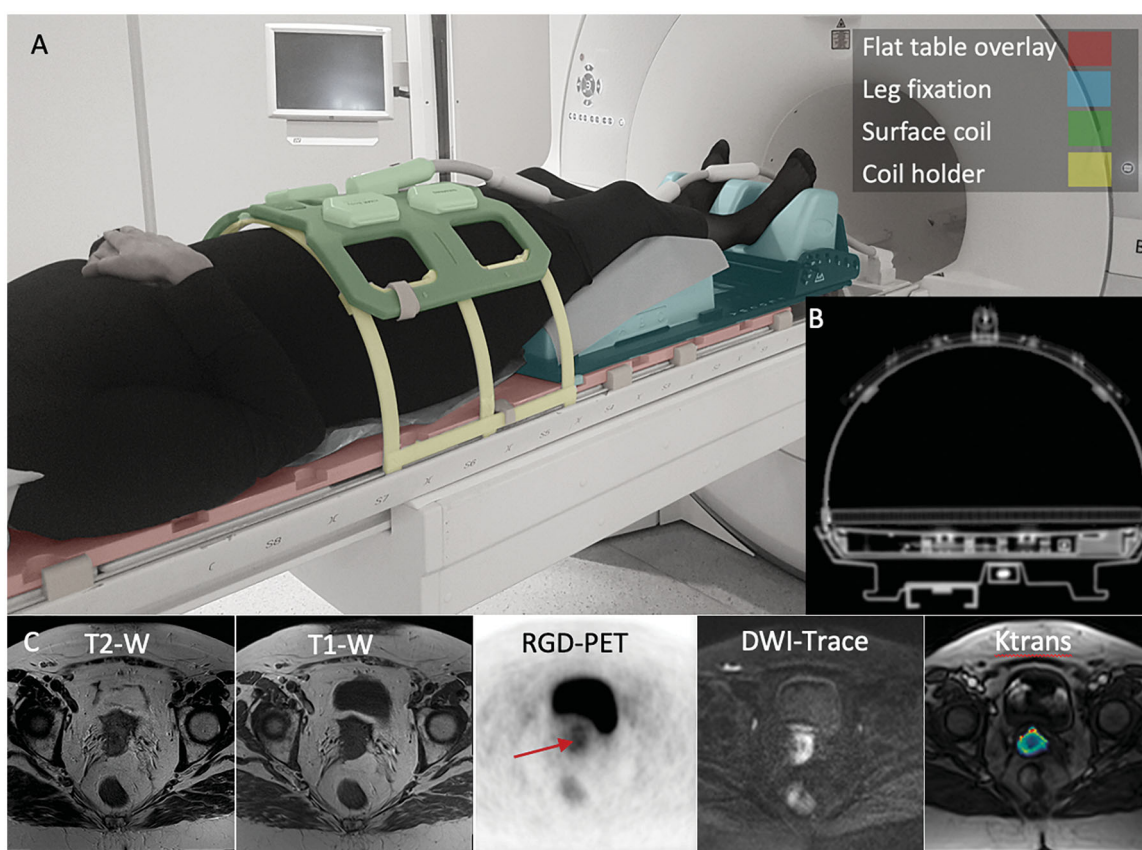


Figure 1. (A) Example of a patient in RT position using dedicated MRI compatible positioning equipment, and (B) generated AC map of RT set-up incorporated into the hardware AC map. (C) A representative multi-parametric PET/MRI image dataset with simultaneous RGD-PET/MRI of a cervical cancer patient.

examination) sequence to provide the AC map. Centralized on the primary tumor, axial DW-MRI and DCE-MRI (with 0.1 ml/kg dosage of gadolinium-DTPA contrast agent) were performed.

An additional PET was acquired over two-bed positions (3 min/bed) together with a Dixon-VIBE sequence to cover regional lymph nodes and the FOV needed for treatment planning. The scan protocol is described in detail in Table 1.

The pilot patients performed the same protocol, only immediately after routine 2-deoxy-2- ^{18}F fluoro-D-glucose (FDG) PET/CT with no additional radiotracer injection. PET/MRI of the GC patients was also acquired after a routine FDG-PET/CT but not in treatment position. Only the Dixon-VIBE sequence from the GC patients was used in the present study.

RT component attenuation map

An attenuation map of stationary hardware components covering the whole axial area within the PET/MRI gantry was provided by the vendor in linear attenuation coefficients (LAC) at 511 keV.

In order to add the equipment into the existing hardware AC map, the approach suggested by Paulus et al. [13] was used. The entire RT overlay, coils and coil holders, with MR visible markers, were CT scanned in a Siemens TruePoint 64 PET/CT scanner as well as in the PET/MRI system. The RT table overlay, attached coils and coil holders were segmented manually on CT images and registered to the MRI to

be added to the right position in PET/MRI hardware AC map. Attenuation values were converted from Hounsfield Units (HU) to linear LAC at 511 keV using standard bi-linear transform method [36]. The image was blurred with a 5 mm Gaussian filter and then integrated into the existing hardware AC map.

PET/MRI distortion

The geometric distortion level was evaluated using a commercially available 2D spatial integrity phantom (Fluke Biomedical, Everett, WA). The grid portion of the phantom was scanned at three different orientations using a T2 weighted TSE sequence (recommended by the phantom manufacturer) as well as a Dixon sequence employed for sCT generation as explained below (see Table 1) with the field of view (FOV) = $350 \times 350 \text{ mm}^2$. Distortion level was assessed by comparing the detected cylinder center location on images with the ground truth as previously described [37]. The spatial integrity analysis tool (ViewRay) was used to obtain the locations of ground truth. The passing condition for geometric distortion of each marker is 1 mm within 100 mm radius and 2 mm within 175 mm radius from the center.

sCT generation: deep learning approach

A deep convolutional neural network (CNN) in U-Net architecture [38] was developed to generate sCT from

Table 1. Detailed Protocols of PET/MRI.

PET	One BP PET (20 min)			Two BP PET (3 min / each)			DCE		
	T1 Dixon VIBE (AC)	T2-W TSE	T1-W TSE	DWI ($b = 0, 1000$) RESOLVE	Field mapping	T1 Dixon VIBE (AC)	TrueFISP	T1 VIBE	T1 VIBE + Gd
Orientation	Axial	Axial	Axial	Axial	Axial	Axial	Axial	Axial	Axial
TR (ms)	3.85	3290	682	4040	266	3.85	382	5.18	5.18
TE (ms)	1.23, 2.46	115	11	55, 80	4.92, 7.38	1.23, 2.46	1.68	1.09	1.09
Matrix size	$312 \times 384 \times 88$	$512 \times 512 \times 83$	$512 \times 512 \times 53$	$120 \times 160 \times 24$	$120 \times 160 \times 24$	$312 \times 384 \times 154$	$412 \times 512 \times 80$	$128 \times 128 \times 16$	$128 \times 128 \times 16$
Pixel size (mm ²)	1.3×1.3	0.48×0.48	0.48×0.48	2.5×2.5	2.5×2.5	1.3×1.3	0.74×0.74	2.5×2.5	2.5×2.5
Slice thickness (mm)	3	3	3	3	5.5	3	5	5	5
Flip angle (°)	10	160	160	180	60	10	45	2, 5, 15, 25	15

Note. VIBE: volumetric interpolated breath-hold; TSE: turbo spin-echo; BP: bed position.

corresponding Dixon in-phase and opposed-phase images. Undesired information, such as table, pillow, and positioning equipment, outside the patient's body, was removed from CT images and replaced with the CT value equivalent to air and CT voxels were subsequently converted from HU to LAC at 511 keV [36]. Rigid image registration was performed with the Dixon in-phase serving as the fixed image. The resulting transform was used for the initialization of non-rigid registration using the freely available registration package, NiftyReg [39]. All images were resampled to 2 mm isotropic voxel size with a 208×256 in-plane resolution. The input to the network was $208 \times 256 \times 16$ voxel tiles of the images with 2 channels.

The TensorFlow software package [40] was used to implement and train the neural network. Transfer learning was performed from a pre-trained model on 811 brain scans [41]. The hyperparameters were optimized and the model was trained using the Adam optimization algorithm with a fixed learning rate of 10^{-5} , batch size of 2, and mean absolute error as loss function.

For the eight study patients, full sCT volumes were predicted with the exact same shape as inputs ($208 \times 256 \times [132, 231]$). Subsequently, the sCT in LAC was converted back to HU.

The generated sCT was compared with the reference CT on a voxel-wise basis. To quantify the accuracy of sCT mean absolute error (MAE) was calculated within the body contours.

Prior to each fraction of EBRT, cone-beam CT (CBCT) is routinely acquired for position verification. The scan is registered to the planning CT using a bone registration algorithm to reduce the setup variation. To study the performance of the generated sCT for patient positioning, CT and sCT were rigidly registered to the patient's first CBCT using the auto-match tool in the Eclipse treatment planning system (Varian Medical Systems Inc). Absolute differences between registrations were calculated in anterior-posterior (AP), left-right (LR), and superior-inferior (SI) direction.

AC of PET using sCT

To evaluate the quality of PET images acquired from the PET/MRI system PET emission data were reconstructed using two different AC maps: Planning CT image registered to the MR image (PET_{CT}), and the proposed deep sCT (PET_{sCT}). PET volumes were reconstructed using the 3D OSEM algorithm, 3 iterations and 21 subsets, a Gaussian filter with 4 mm full width at half maximum (FWHM), and a 344×344 image matrix. Images were reconstructed with random and absolute scatter correction techniques.

The accuracy of PET_{sCT} was compared with PET_{CT} as a reference by measuring the SUV_{max} and SUV_{mean} values within the tumor volume. A threshold of 50% of the maximum SUV was selected for outlining the tumor volume.

Dose calculation using sCT

Study patients were planned for volumetric modulated arc therapy (VMAT) using Eclipse. Double-arc VMAT plan using

6 MV X-ray beams was created to deliver 45 Gy/25 fractions (1.8 Gy per fraction) to the planning target volume (PTV). To evaluate the performance of sCT for dose calculation, target volume delineations, as well as delineations of OAR, were transferred to the sCT. The treatment plan optimized on planning CT was copied to the sCT and a forward 3D dose distribution within the body contour was performed accordingly. The Acuros XB (version 13.7.14) dose calculation algorithm was configured using the reference dataset.

Dose-volume histogram (DVH) were exported for the target volumes and different OAR. The comparison between sCT and planning CT dose distributions was performed by evaluating mean and maximum absorbed dose (D_{mean} , D_{max}) or the dose delivered to $X\%$ of the volume ($D_{X\%}$) including PTV, sigmoid, and bowel.

In addition, the voxel-wise relative difference map of dose distribution between plans was computed within body contour, PTV, and OAR.

Results

Sixteen patients with an average weight of 75 kg (range: 53–101 kg) underwent PET/MRI using the RT positioning equipment as shown in Figure 1(A). The smaller coil holder, provided by the vendor, could fit on 10 patients and the remaining patients could be scanned using the custom-made coil holder with larger size without any discomfort. The scan protocol was optimized using 8 pilot patients and the study patients with cervical cancer referred for RT treatment were examined using the entire scan protocol. Figure 1(C) shows an example of acquired multiparametric images. The quality of the anatomical MRI images was evaluated by an oncologist and a radiologist confirming suitability for RT delineations in the clinical workflow. The quality of the PET images was evaluated by an experienced, board-certified nuclear medicine physician and tracer uptake in tumor volume was observed.

The average geometric distortions evaluated for the T2-W images and Dixon images were less than 1 mm. Dixon sequence passed the spatial integrity test with a 100% pass rate under all three orientations. The passing rate for T2-w images was 100% within the 100 mm radius and 100%, 98.2%, and 95.3% within 175 mm radius around the isocenter for axial, sagittal, and coronal images, respectively.

The CT-based attenuation map of the RT setup was generated and incorporated into the hardware AC map as shown in Figure 1(B). sCT of volumes for the eight study patients were generated using the trained network. Figure 2(A) shows the sCT compared to planning CT for three subjects in different orientations. According to the error map, the sCT was very similar to the CT, but slightly blurred, with a mean absolute error of 23.7 ± 41.3 HU across the body contour. The absolute mean difference between registration of CT and sCT to the CBCT was 0.16 ± 0.12 , 0.28 ± 0.18 mm, and 0.25 ± 0.29 mm in AP, LR, and SI direction respectively.

The reconstructed PET images for all patients demonstrated an excellent agreement between SUV values of PET_{sCT} and PET_{CT} within the tumor volume (Figure 2(B)).

To evaluate the performance of sCT for dose calculation, the sCT was generated over two bed positions covering the volume needed for RT planning. Dose calculation was then performed for sCT and compared with the reference as shown in Figure 3(A). The error map demonstrates very good agreement between CT- and sCT-based dose calculation with a mean absolute error of 0.11 ± 0.14 Gy within body contours and 0.17 ± 0.12 Gy within tumor volumes. Higher differences at the edge of the body were observed. An exemplar DVH for a patient in Figure 3(B), shows no relevant difference in calculated dose between sCT and CT for PTV, bladder, sigmoid, bowel, and body contour.

Figure 4 presents the absolute differences between DVH metrics, expressed as doses computed on the CT and sCT for all eight study patients. The mean absolute difference for all metrics considered was below 0.5 Gy in all patients.

Discussion

In this study, we have successfully integrated multiparametric PET/MRI as a potential one-stop shop into the treatment planning workflow of cervical cancer patients. Deep learning inferred sCT from MRI images was employed for attenuation correction of PET images, patient positioning, and radiotherapy dose calculations. The proposed set-up provides logistic benefits for the patient, as well as the potential added value of multiparametric PET/MRI for personalized RT planning.

The use of a dedicated RT setup was feasible in all 16 patients included in the study with a weight of up to 101 kg. The scan protocol was optimized to meet the clinical requirements for RT planning and scan time was less than 45 min including preparation time. The RF coil holder can be placed at different positions along the flat table overlay providing indexation to enable optimum repeatability of patient positioning. Further, the indexing system was used to specify the exact location of the coil holder and facilitate generating a patient-specific AC map of the setup. Several groups have investigated the AC of hardware and RT components for PET/MRI, but with a different setup and for different regions [34,37,42,43]. Paulus et al. [13] developed and tested RT equipment for whole-body PET/MRI, but did not include dedicated RT equipment (coil holder, leg fixation) for imaging of the pelvic region.

We wish to underline that while our setup resulted in clinically acceptable MRI images and accurate PET quantification, our results go beyond previous studies and evaluates the full integration of PET/MRI only for RT treatment planning of cervical cancer patients. To create patient specific electron density map, we generated a sCT very similar to CT, but with a blurred appearance specially in the abdomen which could be the result of respiratory motion and also large voxel size in MRI.

The mean absolute difference between registration of CBCT to CT and sCT was less than 0.3 mm in all directions. The result was in agreement with previous studies suggesting that sCT could be used as a reference for positioning verification and provides an accurate alignment to CBCT [17].

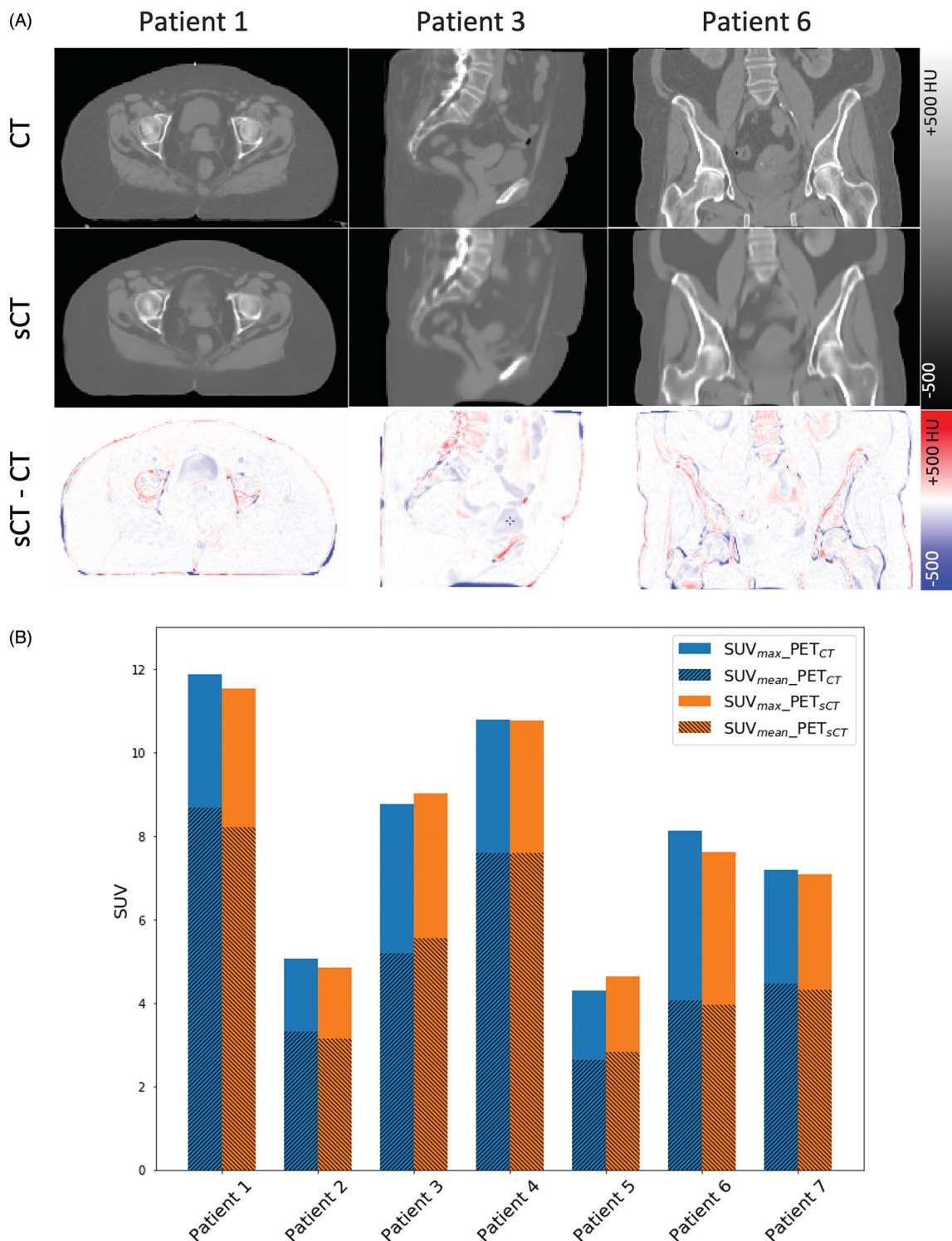


Figure 2. (A) examples of CT and sCT images of three patients in different orientations. (B) Bar graphs comparing SUV_{max} and SUV_{mean} values between PET_{CT} (blue color) and PET_{sCT} (orange color) in tumor volumes.

Comparing CT- and sCT-based AC, our findings show a small difference between two methods, which however did not lead to significant effects on quantification of PET uptake in tumors. Dosimetric evaluation of sCT compared to CT revealed essentially identical dose distributions within the target volume and OAR. The dosimetric error map shows high intensity at the border of the body, which could result

from the apparent slightly lower resolution of the sCT images. On closer inspection of the dose difference maps, a grid pattern can be observed as a result of slight misalignment between CT and sCT. However, the DVH in Figure 3(B) showed a perfect agreement between the plan based on sCT and conventional CT confirming that the sCT can be utilized for treatment planning of cervical cancer patients. Our results

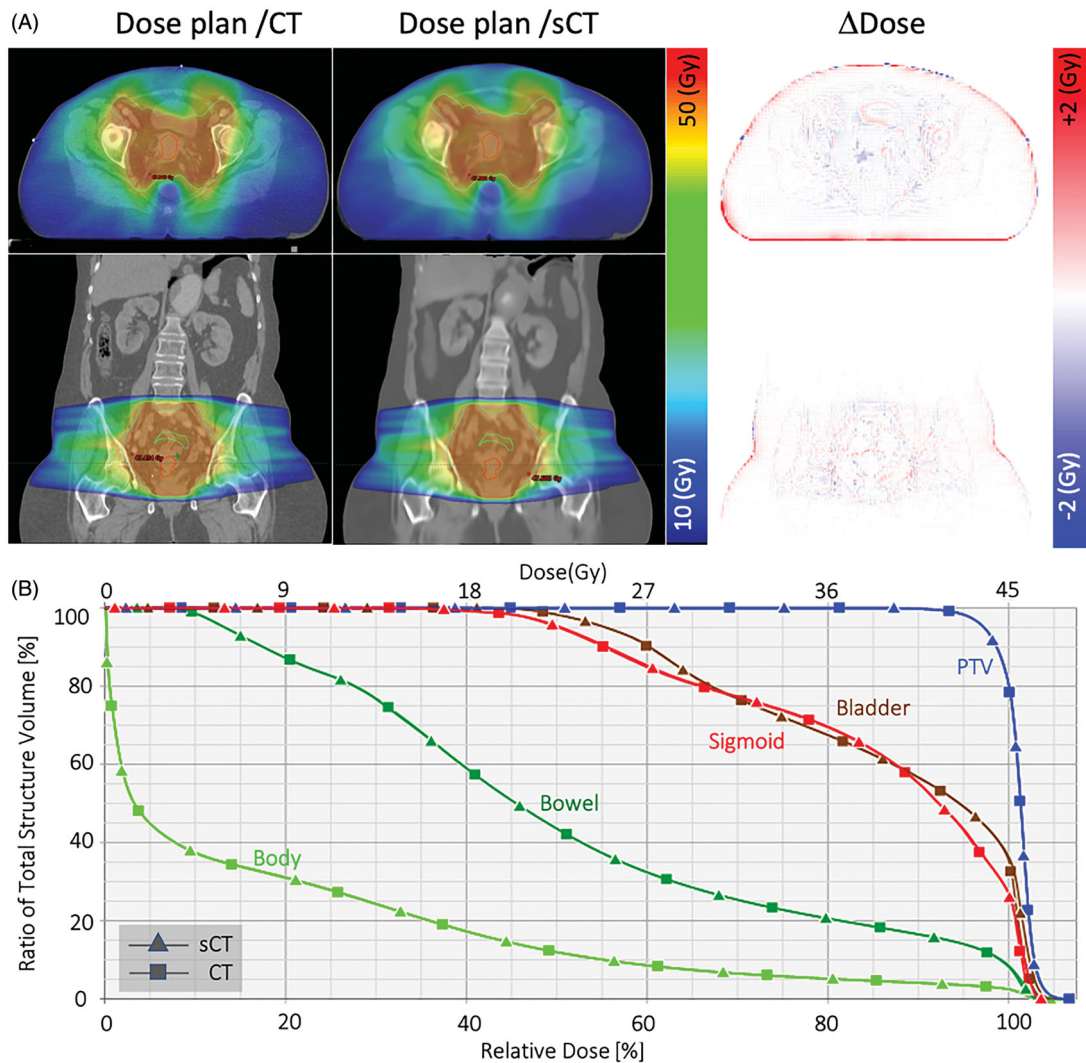


Figure 3. (A) The calculated dose plan for sCT and CT images and the error map representing the dose distribution difference. (B) DVH curve comparing the planned dose of target volumes and different OAR for CT and sCT.

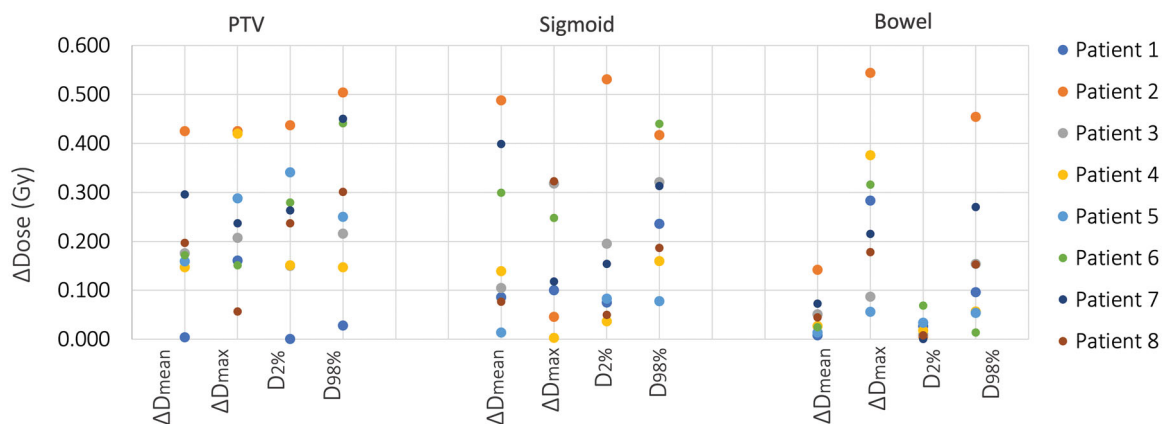


Figure 4. Absolute dose difference between relevant DVH metrics computed on CT and sCT for study patients in PTV, sigmoid and bowel regions.

are comparable to another study [44] which reported 0.4% dose difference in PTV between CT and sCT based dose plans.

In line with previous studies, the error map of the sCT demonstrated some differences at the bone tissue interfaces due to inaccuracies in MRI to CT registration [24,26].

Recently, ZeDD (zero-echo-time and Dixon deep sCT) method has been highlighted for accurate estimation of bony tissues [45]. However, this method comes at the expense of longer acquisition time, while our developed deep learning method relies on Dixon images, which are fast and routine in PET/MRI. Our findings on PET quantification are comparable with

a recent study [26] wherein accurate tumor uptake was observed using sCT for AC. High differences between sCT and CT were observed around the bladder, most likely reflecting that the MRI and CT were acquired at different time points. The sCT, however, is based on a Dixon sequence acquired at the same time point as PET. Thus, it is likely that sCT based AC might be more accurate for this purpose than a separate CT, underscoring the potential of PET/MRI as a one-stop shop.

Geometrical accuracy is important when MRI techniques are used to define the boundaries of a tumor volume [16]. According to the study, geometric accuracy of 1 mm in PTV is desired for MR-guided RT [46]. Based on our phantom measurements, the geometric distortion was within the approved range and less in close proximity to the isocenter. Although it is critical to position the target as close as possible to the isocenter, this is not always feasible in cervical cancer due to the fixed table height. However, in our study, all target volumes were positioned within a 150 mm radius around the isocenter where the geometric distortion was less than 1 mm. Given the small geometric distortion of the Dixon images, dosimetric uncertainties relating to distortion are expected to be very limited.

The accuracy of the generated sCT relies on an ideal alignment between CT and MRI in training data. Given the different positioning between MRI and CT scans for pilot patients and GC patients, some residual registration error remains. In both PET/CT and PET/MRI scans, no positioning equipment has been used for GC patients, while for pilot patients, only PET/MRI was acquired in RT position. Another limitation of the present study is that the network was trained with both contrast and non-contrast CTs, which may cause errors in the predicted sCT map. However, another study [47] evaluated the effect of IV contrast on dose calculation and confirmed that the difference between plans based on contrast and non-contrast CT is clinically insignificant with a relative mean dose of 2%. The accuracy of the sCT is expected to improve with a larger dataset for training. However, it should be noted that it is an inherent property of deep learning-based methods that they can occasionally fail unpredictably in very few patients, despite performing well in the vast majority. We would therefore strongly recommend an independent verification of the sCT algorithm before clinical implementation. Finally, after inclusion and analysis of the 8 patients reported here, a subsequent patient was observed not to fit PET/MR coil holder. The patient had a weight of 137 kg. Hence, the requirements of the RT equipment combined the 60 cm bore size of current integrated PET/MRI systems can be a limitation for some patients.

In future research, we intend to examine the robustness of our results by including more data and demonstrate the potential of improving RT planning by using complementary information acquired from multiparametric data.

Conclusion

This study demonstrates the successful integration of multiparametric PET/MRI for RT planning of patients with cervical

cancer, including dedicated RT equipment and sCT acceptable for PET AC and dose calculation. Hence, the potential of multiparametric imaging for contributing to dose planning can now be evaluated in larger patient groups. The present work may also serve as an inspirational set-up guide for other groups embarking on PET/MRI for improving RT planning in patients with cervical cancer.

Disclosure statement

No potential conflict of interest was reported by the author(s).

Funding

This project has received funding from the European Union's Horizon 2020 research and innovation program under the Marie Skłodowska-Curie Grant [764458].

ORCID

Sahar Ahangari  <http://orcid.org/0000-0002-1561-4684>

Ivan Richter Vogelius  <http://orcid.org/0000-0002-8877-1218>

Barbara Malene Fischer  <http://orcid.org/0000-0002-8361-4678>

References

- [1] Arbyn M, Weiderpass E, Bruni L, et al. Estimates of incidence and mortality of cervical cancer in 2018: a worldwide analysis. *Lancet Glob Heal*. 2020;8(2):e191–e203.
- [2] Vordermark D. Radiotherapy of cervical cancer. *Oncol Res Treat*. 2016;39(9):516–520.
- [3] Tan ML, Tanderup K, Kirisits C, et al. Image-guided adaptive radiotherapy in cervical cancer. *Semin Radiat Oncol*. 2019;29(3):284–298.
- [4] Van De Bunt L, Van Der Heide UA, Ketelaars M, et al. Conventional, conformal, and intensity-modulated radiation therapy treatment planning of external beam radiotherapy for cervical cancer: The impact of tumor regression. *Int J Radiat Oncol Biol Phys*. 2006;64(1):189–196.
- [5] Sasidharan A, Mahantshetty UM, Gurram L, et al. Patterns of first relapse and outcome in patients with locally advanced cervical cancer after radiochemotherapy: a single institutional experience. *Indian J Gynecol Oncol*. 2020;18:3–8.
- [6] Forrest J, Presutti J, Davidson M, et al. A dosimetric planning study comparing intensity-modulated radiotherapy with four-field conformal pelvic radiotherapy for the definitive treatment of cervical carcinoma. *Clin Oncol*. 2012;24(4):e63–e70.
- [7] Azria D, Lapierre A, Gourgou S, et al. Data-based radiation oncology: Design of clinical trials in the toxicity biomarkers era. *Front Oncol*. 2017;7:1–11.
- [8] Fields EC, Weiss E. A practical review of magnetic resonance imaging for the evaluation and management of cervical cancer. *Radiat Oncol*. 2016;11(1):10.
- [9] Han K, Croke J, Foltz W, et al. A prospective study of DWI, DCE-MRI and FDG PET imaging for target delineation in brachytherapy for cervical cancer. *Radiother Oncol*. 2016;120(3):519–525.
- [10] Dappa E, Elger T, Hasenburg A, et al. The value of advanced MRI techniques in the assessment of cervical cancer: a review. *Insights Imaging*. 2017;8(5):471–481.
- [11] Daniel M, Andrzejewski P, Sturdza A, et al. Impact of hybrid PET/MR technology on multiparametric imaging and treatment response assessment of cervix cancer. *Radiother Oncol*. 2017;125(3):420–425.

- [12] Thorwarth D, Leibfarth S, Mönnich D. Potential role of PET/MRI in radiotherapy treatment planning. *Clin Transl Imaging*. 2013;1(1):45–51.
- [13] Paulus DH, Oehmigen M, Grüneisen J, et al. Whole-body hybrid imaging concept for the integration of PET/MR into radiation therapy treatment planning. *Phys Med Biol*. 2016;61(9):3504–3520.
- [14] Rausch I, Quick HH, Cal-Gonzalez J, et al. Technical and instrumental foundations of PET/MRI. *Eur J Radiol*. 2017;94:A3–A13.
- [15] Delso G, Fürst S, Jakoby B, et al. Performance measurements of the siemens mMR integrated whole-body PET/MR scanner. *J Nucl Med*. 2011;52(12):1914–1922.
- [16] Walker A, Liney G, Metcalfe P, et al. MRI distortion: Considerations for MRI based radiotherapy treatment planning. *Australas Phys Eng Sci Med*. 2014;37(1):103–113.
- [17] Kempainen R, Suilamo S, Ranta I, et al. Assessment of dosimetric and positioning accuracy of a magnetic resonance imaging-only solution for external beam radiotherapy of pelvic anatomy. *Phys Imaging Radiat Oncol*. 2019;11:1–8.
- [18] Owringi AM, Greer PB, Glide-Hurst CK. MRI-only treatment planning: Benefits and challenges. *Phys Med Biol*. 2018;63:1–30.
- [19] Persson E, Jamtheim Gustafsson C, Ambolt P, et al. MR-PROTECT: Clinical feasibility of a prostate MRI-only radiotherapy treatment workflow and investigation of acceptance criteria. *Radiat Oncol*. 2020;15(1):13.
- [20] Ladefoged CN, Benoit D, Law I, et al. Region specific optimization of continuous linear attenuation coefficients based on UTE (RESOLUTE): Application to PET/MR brain imaging. *Phys Med Biol*. 2015;60(20):8047–8065.
- [21] Sahiner B, Pezeshk A, Hadjiiski LM, et al. Deep learning in medical imaging and radiation therapy. *Med Phys*. 2019;46(1):e1–e36.
- [22] Hsu SH, DuPre P, Peng Q, et al. A technique to generate synthetic CT from MRI for abdominal radiotherapy. *J Appl Clin Med Phys*. 2020;21(2):136–143.
- [23] Palmér E, Karlsson A, Nordström F, et al. Synthetic computed tomography data allows for accurate absorbed dose calculations in a magnetic resonance imaging only workflow for head and neck radiotherapy. *Phys Imaging Radiat Oncol*. 2021;17:36–42.
- [24] Bradshaw TJ, Zhao G, Jang H, et al. Feasibility of deep learning-based PET/MR attenuation correction in the pelvis using only diagnostic MR images. *Tomogr*. 2018;4(3):138–147.
- [25] Arabi H, Dowling JA, Burgos N, et al. Comparative study of algorithms for synthetic CT generation from MRI: Consequences for MRI-guided radiation planning in the pelvic region. *Med Phys*. 2018;45(11):5218–5233.
- [26] Torrado-Carvajal A, Vera-Olmos J, Izquierdo-Garcia D, et al. Dixon-vibe deep learning (divide) pseudo-CT synthesis for pelvis PET/MR attenuation correction. *J Nucl Med*. 2019;60(3):429–435.
- [27] Bahrami A, Karimian A, Fatemizadeh E, et al. A new deep convolutional neural network design with efficient learning capability: Application to CT image synthesis from MRI. *Med Phys*. 2020;47(10):5158–5171.
- [28] Bird D, Henry AM, Sebag-Montefiore D, et al. A systematic review of the clinical implementation of pelvic magnetic resonance imaging-only planning for external beam radiation therapy. *Int J Radiat Oncol Biol Phys*. 2019;105(3):479–492.
- [29] Siversson C, Nordström F, Nilsson T, et al. Technical note: MRI only prostate radiotherapy planning using the statistical decomposition algorithm. *Med Phys*. 2015;42(10):6090–6097.
- [30] Pozaruk A, Pawar K, Li S, et al. Augmented deep learning model for improved quantitative accuracy of MR-based PET attenuation correction in PSMA PET-MRI prostate imaging. *Eur J Nucl Med Mol Imaging*. 2021;48(1):9–20.
- [31] Leynes AP, Yang J, Shanbhag DD, et al. Hybrid ZTE/Dixon MR-based attenuation correction for quantitative uptake estimation of pelvic lesions in PET/MRI. *Med Phys*. 2017;44(3):902–913.
- [32] Eldib M, Bini J, Faul DD, et al. Attenuation correction for magnetic resonance coils in combined PET/MR imaging: a review. *PET Clin*. 2016;11(2):151–160.
- [33] Mantlik F, Hofmann M, Werner MK, et al. The effect of patient positioning aids on PET quantification in PET/MR imaging. *Eur J Nucl Med Mol Imaging*. 2011;38(5):920–929.
- [34] Paulus DH, Thorwarth D, Schmidt H, et al. Towards integration of PET/MR hybrid imaging into radiation therapy treatment planning. *Med Phys*. 2014;41(7):72505.
- [35] Oxboel J, Brandt-Larsen M, Schjoeth-Eskesen C, et al. Comparison of two new angiogenesis PET tracers 68Ga-NODAGA-E[c(RGDyK)]₂ and (64)Cu-NODAGA-E[c(RGDyK)]₂; in vivo imaging studies in human xenograft tumors. *Nucl Med Biol*. 2014;41(3):259–267.
- [36] Carney JPJ, Townsend DW, Rappoport V, et al. Method for transforming CT images for attenuation correction in PET/CT imaging. *Med Phys*. 2006;33(4):976–983.
- [37] Olin AB, Hansen AE, Rasmussen JH, et al. Feasibility of multiparametric positron emission tomography/magnetic resonance imaging as a one-stop shop for radiation therapy planning for patients with head and neck cancer. *Int J Radiat Oncol Biol Phys*. 2020;108(5):1329–1338.
- [38] Ronneberger O, Fischer P, Brox T. U-net: convolutional networks for biomedical image segmentation. *Lect Notes Comput Sci*. 2015;9351:234–241.
- [39] Modat M, Ridgway GR, Taylor ZA, et al. Fast free-form deformation using graphics processing units. *Comput Methods Programs Biomed*. 2010;98(3):278–284.
- [40] Abadi M, Barham P, Chen J, et al. TensorFlow: a system for large-scale machine learning. 12th USENIX Symposium on Operating Systems Design and Implementation (OSDI 16). 2016;265–283.
- [41] Ladefoged CN, Hansen AE, Henriksen OM, et al. AI-driven attenuation correction for brain PET/MRI: Clinical evaluation of a dementia cohort and importance of the training group size. *Neuroimage*. 2020;222:117221.
- [42] Witoszynskij S, Andrzejewski P, Georg D, et al. Attenuation correction of a flat table top for radiation therapy in hybrid PET/MR using CT- and 68Ge/68Ga transmission scan-based μ -maps. *Phys Med*. 2019;65:76–83.
- [43] Winter RM, Leibfarth S, Schmidt H, et al. Assessment of image quality of a radiotherapy-specific hardware solution for PET/MRI in head and neck cancer patients. *Radiother Oncol*. 2018;128(3):485–491.
- [44] Farjam R, Tyagi N, Deasy JO, et al. Dosimetric evaluation of an atlas-based synthetic CT generation approach for MR-only radiotherapy of pelvis anatomy. *J Appl Clin Med Phys*. 2019;20(1):101–109.
- [45] Leynes AP, Yang J, Wiesinger F, et al. Zero-echo-time and dixon deep pseudo-CT (ZeDD CT): direct generation of pseudo-CT images for pelvic PET/MRI attenuation correction using deep convolutional neural networks with multiparametric MRI. *J Nucl Med*. 2018;59(5):852–858.
- [46] Weygand J, Fuller CD, Ibbott GS, et al. Spatial precision in magnetic resonance imaging-guided radiation therapy: the role of geometric distortion. *Int J Radiat Oncol Biol Phys*. 2016;95(4):1304–1316.
- [47] Heydarheydari S, Farshchian N, Haghparast A. Influence of the contrast agents on treatment planning dose calculations of prostate and rectal cancers. *Reports Pract Oncol Radiother*. 2016;21(5):441–446.